Tritium distributions on W-coated divertor tiles used in the third JET ITER-like wall campaign

Eriksson, F.; Eriksson, J.; Eriksson, L. G.; Esposito, B.; Esquembri, S.; Esser, H. G.; Esteve, D.; Evans, B.; Evans, G. E.; Evison, G.; Ewart, G. D.; Fagan, D.; Faitsch, M.; Falie, D.; Fanni, A.; Fasoli, A.; Faustin, J. M.; Fawlk, N.; Fazendeiro, L.; Fedorczak, N.; Felton, R. C.; Fenton, K.; Fernades, A.; Fernandes, H.; Ferreira, J.; Fessey, J. A.; Fevrier, O.; Ficker, O.; Field, A.; Fietz, S.; Figueiredo, A.; Figueiredo, J.; Fil, A.; Finburg, P.; Firdaouss, M.; Fischer, U.; Fittill, L.; Fitzgerald, M.; Flammini, D.; Flanagan, J.; Fleming, C.; Flinders, K.; Fonnesu, N.; Fontdecaba, J. M.; Formisano, A.; Forsythe, L.; Fortuna, L.; Fortuna-Zalesna, E.; Fortune, M.; Foster, S.; Franke, T.; Franklin, T.; Frasca, M.; Frassinetti, L.; Freisinger, M.; Fresa, R.; Frigione, D.; Fuchs, V.; Fuller, D.; Futatani, S.; Fyvie, J.; Gal, K.; Galassi, D.; Galazka, K.; Galdon-Quiroga, J.; Gallagher, J.; Gallart, D.; Galvao, R.; Gao, X.; Gao, Y.; Garcia, J.; Garcia-Carrasco, A.; Garcia-Munoz, M.; Gardarein, J. L.; Garzotti, L.; Gaudio, P.; Gauthier, E.; Gear, D. F.; Gee, S. J.; Geiger, B.; Gelfusa, M.; Gerasimov, S.; Gervasini, G.; Gethins, M.; Ghani, Z.; Ghate, M.; Gherendi, M.; Giacalone, J. C.; Giacomelli, L.; Gibson, C. S.; Giegerich, T.; Gil, C.; Gil, L.; Gilligan, S.; Gin, D.; Giovannozzi, E.; Girardo, J. B.; Giroud, C.; Giruzzi, G.; Gloeggler, S.; Godwin, J.; Goff, J.; Gohil, P.; Goloborod'Ko, V.; Gomes, R.; Goncalves, B.; Goniche, M.; Goodliffe, M.; Goodyear, A.; Gorini, G.; Gosk, M.; Goulding, R.; Goussarov, A.; Gowland, R.; Graham, B.; Graham, M. E.; Graves, J. P.; Grazier, N.; Grazier, P.; Green, N. R.; Greuner, H.; Grierson, B.; Griph, F. S.; Grisolia, C.; Grist, D.; Groth, M.; Grove, R.; Grundy, C. N.; Grzonka, J.; Guard, D.; Guerard, C.; Guillemaut, C.; Guirlet, R.; Gurl, C.; Utoh, H. H.; Hackett, L. J.; Hacquin, S.; Hagar, A.; Hager, R.; Hakola, A.; Halitovs, M.; Hall, S. J.; Hallworth Cook, S. P.; Hamlyn-Harris, C.; Hammond, K.; Harrington, C.; Harrison, J.; Harting, D.; Hasenbeck, F.; Hatch, D. R.; Haupt, V.; Hawes, T. D. J.; Hawkes, N. C.; Hawkins, J.; Hawkins, P.; Haydon, P. W.; Hayter, N.; Hazel, S.; Heesterman, P. J. L.; Heinola, K.; Hellesen, C.; Hellsten, T.; Helou, W.; Hemming, O. N.; Hender, T. C.; Henderson, M.; Henderson, S. S.; Henriques, R.; Hepple, D.; Hermon, G.; Hertout, P.; Hidalgo, C.; Highcock, E. G.; Hill, M.; Hillairet, J.; Hillesheim, J.; Hillis, D.; Hizanidis, K.; Hjalmarsson, A.; Hobirk, J.; Hodille, E.; Hogben, C. H. A.; Hogeweij, G. M. D.; Hollingsworth, A.; Hollis, S.; Homfray, D. A.; Horcek, J.; Hornung, G.; Horton, A. R.; Horton, L. D.; Horvath, L.; Hotchin, S. P.; Hough, M. R.; Howarth, P. J.; Hubbard, A.; Huber, A.; Huber, V.; Huddleston, T. M.; Hughes, M.; Huijsmans, G. T. A.; Hunter, C. L.; Huynh, P.; Hynes, A. M.; Iglesias, D.; Imazawa, N.; Imbeaux, F.; Imrisek, M.; Incelli, M.; Innocente, P.; Irishkin, M.; Ivanova-Stanik, I.; Jachmich, S.; Jacobsen, A. S.; Jacquet, P.; Jansons, J.; Jardin, A.; Jarvinen, A.; Jaulmes, F.; Jednorog, S.; Jenkins, I.; Jeong, C.; Jepu, I.; Joffrin, E.; Johnson, R.; Johnson, T.; Johnston, J.; Joita, L.; Jones, G.; Jones, T. T. C.; Hoshino, K. K.; Kallenbach, A.; Kamiya, K.; Kaniewski, J.; Kantor, A.; Kappatou, A.; Karhunen, J.; Karkinsky, D.; Karnowska, I.; Kaufman, M.; Kaveney, G.; Kazakov, Y.; Kazantzidis, V.; Keeling, D. L.; Keenan, T.; Keep, J.; Kempenaars, M.; Kennedy, C.; Kenny, D.; Kent, J.; Kent, O. N.; Khilkevich, E.; Kim, H. T.; Kim, H. S.; Kinch, A.; King, C.; King, D.; King, R. F.; Kinna, D. J.; Kiptily, V.; Kirk, A.; Kirov, K.; Kirschner, A.; Kizane, G.; Klepper, C.; Klix, A.; Knight, P.; Knipe, S. J.; Knott, S.; Kobuchi, T.; Koechl, F.; Kocsis, G.; Kodeli, I.; Kogan, L.; Kogut, D.; Kominis, Y.; Koeppen, M.; Kos, B.; Koskela, T.; Koslowski, H. R.; Koubiti, M.; Kovari, M.; Kowalska-Strzeciwilk, E.; Krasilnikov, A.; Krasilnikov, V.; Krawczyk, N.; Kresina, M.; Krieger, K.; Krivska, A.; Kruezi, U.; Ksiazek, I.; Kukushkin, A.; Kundu, A.; Kurki-Suonio, T.; Kwak, S.; Kwiatkowski, R.; Kwon, O. J.; Laguardia, L.; Lahtinen, A.; Laing, A.; Lam, N.; Lambertz, H. T.; Lane, C.; Lang, P. T.; Lanthaler, S.; Lapins, J.; Lasa, A.; Last, J. R.; Laszynska, E.; Lawless, R.; Lawson, A.; Lawson, K. D.; Lazaros, A.; Lazzaro, E.; Leddy, J.; Lee, S.; Lefebvre, X.; Leggate, H. J.; Lehmann, J.; Lehnen, M.; Leichtle, D.; Leichuer, P.; Leipold, F.; Lengar, I.; Lennholm, M.; Lerche, E.; Lescinskis, A.; Lesnoj, S.; Letellier, E.; Leyland, M.; Leysen, W.; Li, L.; Liang, Y.; Linke, J.; Linsmeier, C.; Lipschultz, B.; Liu, G.; Liu, Y.; Lo Schiavo, V. P.; Loarer, T.; Loarte, A.; Lobel, R. C.; Lomanowski, B.; Lomas, P. J.; Lonnroth, J.; Lopez, J. M.; Lopez-Razola, J.; Lorenzini, R.; Losada, U.; Lovell, J. J.; Loving, A. B.; Lowry, C.; Luce, T.; Lucock, R. M. A.; Lukin, A.; Luna, C.; Lungaroni, M.; Lungu, C. P.; Lungu, M.; Lunniss, A.; Lupelli, I.; Lyssoivan, A.; Macdonald, N.; Macheta, P.; Maczewa, K.; Magesh, B.; Maget, P.; Maggi, C.; Maier, H.; Mailloux, J.; Makkonen, T.; Makwana, R.; Malaquias, A.; Malizia, A.; Manas, P.; Manning, A.; Manso, M. E.; Mantica, P.; Mantsinen, M.; Manzanares, A.; Maquet, P.; Marandet, Y.; Marcenko, N.; Marchetto, C.; Marchuk, O.; Marinelli, M.; Marinucci, M.; Markovic, T.; Marocco, D.; Marot, L.; Marren, C. A.; Marshal, R.; Martin, A.; Martin, Y.; Martin de Aguilera, A.; Martinez, F. J.; Martin-Sols, J. R.; Martynova, Y.; Maruyama, S.; Masiello, A.; Maslov, M.; Matejcik, S.; Mattei, M.; Matthews, G. F.; Maviglia, F.; Mayer, M.; Mayoral, M. L.; May-Smith, T.; Mazon, D.; Mazzotta, C.; Mcadams, R.; Mccarthy, P. J.; Mcclements, K. G.; Mccormack, O.; Mccullen, P. A.; Mcdonald, D.; Mcintosh, S.; Mckean, R.; Mckehon, J.; Meadows, R. C.; Meakins, A.; Medina, F.; Medland, M.; Medley, S.; Meigh, S.; Meigs, A. G.; Meisl, G.; Meitner, S.; Meneses, L.; Menmuir, S.; Mergia, K.; Merrigan, I. R.; Mertens, P.; Meshchaninov, S.; Messiaen, A.; Meyer, H.; Mianowski, S.; Michling, R.; Middleton-Gear, D.; Miettunen, J.; Militello, F.; Militello-Asp, E.; Miloshevsky, G.; Mink, F.; Minucci, S.; Miyoshi, Y.; Mlynar, J.; Molina, D.; Monakhov, I.; Moneti, M.; Mooney, R.; Moradi, S.; Mordijck, S.; Moreira, L.; Moreno, R.; Moro, F.; Morris, A. W.; Morris, J.; Moser, L.; Mosher, S.; Moulton, D.; Murari, A.; Muraro, A.; Murphy, S.; Asakura, N. N.; Na, Y. S.; Nabais, F.; Naish, R.; Nakano, T.; Nardon, E.; Naulin, V.; Nave, M. F. F.; Nedzelski, I.; Nemtsev, G.; Nespoli, F.; Neto, A.; Neu, R.; Neverov, V. S.; Newman, M.; Nicholls, K. J.; Nicolas, T.; Nielsen, A. H.; Nielsen, P.; Nilsson, E.; Nishijima, D.; Noble, C.; Nocente, M.; Nodwell, D.; Nordlund, K.; Nordman, H.; Nouailletas, R.; Nunes, I.; Oberkofler, M.; Odupitan, T.; Ogawa, M. T.; O'Gorman, T.; Okabayashi, M.; Olney, R.; O'Molayo, O.; Omullane, M.; Ongena, J.; Orsitto, F.; Orszagh, J.; Oswuigwe, I.; Otin, B. R.; Owen, A.; Paccagnella, R.; Pace, N.; Pacella, D.; Packer, L. W.; Page, A.; Pajuste, E.; Palazzo, S.; Pamela, S.; Panja, S.; Papp, P.; Paprok, R.; Parail, V.; Park, M.; Parra Diaz, F.; Parsons, M.; Pasqualotto, R.; Patel, A.; Pathak, S.; Paton, D.; Patten, H.; Pau, A.; Pawelec, E.; Paz Soldan, C.; Peackoc, A.; Pearson, I. J.; Pehkonen, S. P.; Peluso, E.; Penot, C.; Pereira, A.; Pereira, R.; Pereira Puglia, P. P.; Perez von Thun, C.; Peruzzo, S.; Peschanyi, S.; Peterka, M.; Petersson, P.; Petravich, G.; Petre, A.; Petrella, N.; Petrzilka, V.; Peysson, Y.; Pfefferle, D.; Philipps, V.; Pillon, M.; Pintsuk, G.; Piovesan, P.; Pires dos Reis, A.;

Piron, L.; Pironti, A.; Pisano, F.; Pitts, R.; Pizzo, F.; Plyusnin, V.; Pomaro, N.; Pompilian, O. G.; Pool, P. J.; Popovichev, S.; Porfiri, M. T.; Porosnicu, C.; Porton, M.; Possnert, G.; Potzel, S.; Powell, T.; Pozzi, J.; Prajapati, V.; Prakash, R.; Prestopino, G.; Price, D.; Price, M.; Price, R.; Prior, P.; Proudfoot, R.; Pucella, G.; Puglia, P.; Puiatti, M. E.; Pulley, D.; Purahoo, K.; Puetterich, T.; Rachlew, E.; Rack, M.; Ragona, R.; Rainford, M. S. J.; Rakha, A.; Ramogida, G.; Ranjan, S.; Rapson, C. J.; Rasmussen, J. J.; Rathod, K.; Ratta, G.; Ratynskaia, S.; Ravera, G.; Rayner, C.; Rebai, M.; Reece, D.; Reed, A.; Refy, D.; Regan, B.; Regana, J.; Reich, M.; Reid, N.; Reimold, F.; Reinhart, M.; Reinke, M.; Reiser, D.; Rendell, D.; Reux, C.; Reyes Cortes, S. D. A.; Reynolds, S.; Riccardo, V.; Richardson, N.; Riddle, K.; Rigamonti, D.; Rimini, F. G.; Risner, J.; Riva, M.; Roach, C.; Robins, R. J.; Robinson, S. A.; Robinson, T.; Robson, D. W.; Roccella, R.; Rodionov, R.; Rodrigues, P.; Rodriguez, J.; Rohde, V.; Romanelli, F.; Romanelli, M.; Romanelli, S.; Romazanov, J.; Rowe, S.; Rubel, M.; Rubinacci, G.; Rubino, G.; Ruchko, L.; Ruiz, M.; Ruset, C.; Rzadkiewicz, J.; Saarelma, S.; Sabot, R.; Safi, E.; Sagar, P.; Saibene, G.; Saint-Laurent, F.; Salewski, M.; Salmi, A.; Salmon, R.; Salzedas, F.; Samaddar, D.; Samm, U.; Sandiford, D.; Santa, P.; Santala, M. I. K.; Santos, B.; Santucci, A.; Sartori, F.; Sartori, R.; Sauter, O.; Scannell, R.; Schlummer, T.; Schmid, K.; Schmidt, V.; Schmuck, S.; Schneider, M.; Schoepf, K.; Schworer, D.; Scott, S. D.; Sergienko, G.; Sertoli, M.; Shabbir, A.; Sharapov, S. E.; Shaw, A.; Shaw, R.; Sheikh, H.; Shepherd, A.; Shevelev, A.; Shumack, A.; Sias, G.; Sibbald, M.; Sieglin, B.; Silburn, S.; Silva, A.; Silva, C.; Simmons, P. A.; Simpson, J.; Simpson-Hutchinson, J.; Sinha, A.; Sipila, S. K.; Sips, A. C. C.; Siren, P.; Sirinelli, A.; Sjostrand, H.; Skiba, M.; Skilton, R.; Slabkowska, K.; Slade, B.; Smith, N.; Smith, P. G.; Smith, R.; Smith, T. J.; Smithies, M.; Snoj, L.; Soare, S.; Solano, E. R.; Somers, A.; Sommariva, C.; Sonato, P.; Sopplesa, A.; Sousa, J.; Sozzi, C.; Spagnolo, S.; Spelzini, T.; Spineanu, F.; Stables, G.; Stamatelatos, I.; Stamp, M. F.; Staniec, P.; Stankunas, G.; Stan-Sion, C.; Stead, M. J.; Stefanikova, E.; Stepanov, I.; Stephen, V.; Stephen, A. M.; Stevens, A.; Stevens, B. D.; Strachan, J.; Strand, P.; Strauss, H. R.; Strom, P.; Stubbs, G.; Studholme, W.; Subba, F.; Summers, H. P.; Svensson, J.; Swiderski, L.; Szabolics, T.; Szawlowski, M.; Szepesi, G.; Suzuki, T. T.; Tal, B.; Tala, T.; Talbot, A. R.; Talebzadeh, S.; Taliercio, C.; Tamain, P.; Tame, C.; Tang, W.; Tardocchi, M.; Taroni, L.; Taylor, D.; Taylor, K. A.; Tegnered, D.; Telesca, G.; Teplova, N.; Terranova, D.; Testa, D.; Tholerus, E.; Thomas, J.; Thomas, J. D.; Thomas, P.; Thompson, A.; Thompson, C. A.; Thompson, V. K.; Thorne, L.; Thornton, A.; Thrysoe, A. S.; Tigwell, P. A.; Tipton, N.; Tiseanu, I.; Tojo, H.; Tokitani, M.; Tolias, P.; Tomes, M.; Tonner, P.; Towndrow, M.; Trimble, P.; Tripsky, M.; Tsalas, M.; Tsavalas, P.; Tskhakaya Jun, D.; Turner, I.; Turner, M. M.; Turnyanskiy, M.; Tvalashvili, G.; Tyrrell, S. G. J.; Uccello, A.; Ul-Abidin, Z.; Uljanovs, J.; Ulyatt, D.; Urano, H.; Uytdenhouwen, I.; Vadgama, A. P.; Valcarcel, D.; Valentinuzzi, M.; Valisa, M.; Vallejos Olivares, P.; Valovic, M.; Van De Mortel, M.; Van Eester, D.; Van Renterghem, W.; van Rooij, G. J.; Varje, J.; Varoutis, S.; Vartanian, S.; Vasava, K.; Vasilopoulou, T.; Vega, J.; Verdoolaege, G.; Verhoeven, R.; Verona, C.; Verona Rinati, G.; Veshchev, E.; Vianello, N.; Vicente, J.; Viezzer, E.; Villari, S.; Villone, F.; Vincenzi, P.; Vinyar, I.; Viola, B.; Vitins, A.; Vizvary, Z.; Vlad, M.; Voitsekhovitch, I.; Vondracek, P.; Vora, N.; Vu, T.; Pires de Sa, W. W.; Wakeling, B.; Waldon, C. W. F.; Walkden, N.; Walker, M.; Walker, R.; Walsh, M.; Wang, E.; Wang, N.; Warder, S.; Warren, R. J.; Waterhouse, J.; Watkins, N. W.; Watts, C.; Wauters, T.; Weckmann, A.; Weiland, J.; Weisen, H.; Weiszflog, M.; Wellstood, C.; West, A. T.; Wheatley, M. R.; Whetham, S.; Whitehead, A. M.; Whitehead, B. D.; Widdowson, A. M.; Wiesen, S.; Wilkinson, J.; Williams, J.; Williams, M.; Wilson, A. R.; Wilson, D. J.; Wilson, H. R.; Wilson, J.; Wischmeier, M.; Withenshaw, G.; Withycombe, A.; Witts, D. M.; Wood, D.; Wood, R.; Woodley, C.; Wray, S.; Wright, J.; Wright, J. C.; Wu, J.; Wukitch, S.; Wynn, A.; Xu, T.; Yadikin, D.; Yanling, W.; Yao, L.; Yavorskij, V.; Yoo, M. G.; Young, C.; Young, D.; Young, I. D.; Young, R.; Zacks, J.; Zagorski, R.; Zaitsev, F. S.; Zanino, R.; Zarins, A.; Zastrow, K. D.; Zerbini, M.; Zhang, W.; Zhou, Y.; Zilli, E.; Zoita, V.; Zoletnik, S.; Zychor, I.. - In: NUCLEAR MATERIALS AND ENERGY. - ISSN 2352-1791. - 18:(2019), pp. 258-261. [10.1016/j.nme.2019.01.001]

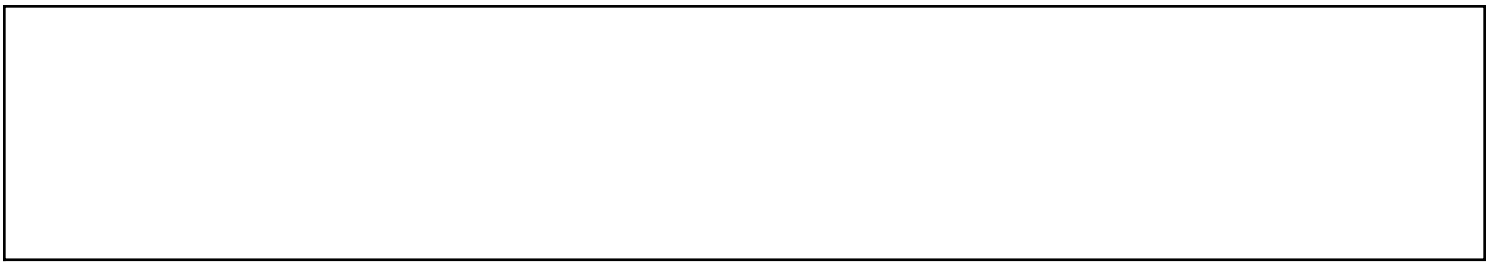

Nuclear Materials and Energy 18 (2019) 258–261

Contents lists available at ScienceDirect

Nuclear Materials and Energy

journal homepage: www.elsevier.com/locate/nme

Tritium distributions on W-coated divertor tiles used in the third JET ITER-like wall campaign

Y. Hatano[a,*], S.E. Lee[a], J. Likonen[b], S. Koivuranta[b], M. Hara[a], S. Masuzaki[c], N. Asakura[d], K. Isobe[d], T. Hayashi[d], J. Ikonen[e], A. Widdowson[f], JET contributors[g,1]

[a] University of Toyama, Toyama 930-8555, Japan
[b] VTT Technical Research Centre of Finland, P. O. Box 1000, FI-02044 VTT, Finland
[c] National Institute for Fusion Science, Toki 509-5292, Japan
[d] National Institutes for Quantum and Radiological Science and Technology, Rokkasho 039-3212, Japan
[e] University of Helsinki, A. I. Virtasen aukio 1, P. O. Box 55, FI-00014, Finland
[f] Culham Centre for Fusion Energy, Culham Science Centre, Abingdon OX14 3DB, UK
[g] EUROfusion Consortium, JET, Culham Science Centre, Abingdon OX14 3DB, UK

ARTICLE INFO

Keywords:
Divertor
Tritium
Retention
Deposition
Radiation

ABSTRACT

Tritium (T) distributions on tungsten (W)-coated plasma-facing tiles used in the third ITER-like wall campaign (2015–2016) of the Joint European Torus (JET) were examined by means of an imaging plate technique and β-ray induced x-ray spectrometry, and they were compared with the distributions after the second (2013–2014) campaign. Strong enrichment of T in beryllium (Be) deposition layers was observed after the second campaign. In contrast, T distributions after the third campaign was more uniform though Be deposition layers were visually recognized. The one of the possible explanations is enhanced desorption of T from Be deposition layers due to higher tile temperatures caused by higher energy input in the third campaign.

1. Introduction

The Joint European Torus (JET) performed three ITER-like Wall (ILW) campaigns with beryllium (Be) main chamber walls and divertor region made of bulk W and W-coated carbon-fiber composite (CFC) tiles in 2011–2012 (ILW-1), 2013–2014 (ILW-2) and 2015–2016 (ILW-3) [1,2]. The characteristics of ILW-3 in comparison with ILW-1 and -2 are its longer period and more high power deuterium (D) discharges [3]; the input energy in ILW-1, -2 and -3 is 150, 201 and 245 GJ, respectively [4]. The inner strike point was predominantly on the surface of inner vertical tile (Tile 3) for ILW-1 and the corner of inner floor tile (Tile 4) for ILW-2, while the outer strike point was predominantly on bulk W Tile 5 for ILW-1 and the corner of outer floor tile (Tile 6) for ILW-2. The distribution of the strike point in ILW-3 was similar to that in ILW-2 [2].

Tritium (T) formed by DD fusion reactions (D + D → 1.01 MeV T + 3.03 MeV p where p is proton) is present in the JET vacuum vessel. A part of T formed is expected to be thermalized in the plasma, while remaining part could be implanted into walls at high energy. Hatano et al. [5,6] have examined the T distribution on the divertor tiles retrieved after ILW-1 by measuring β-rays from T using an imaging plate (IP) technique. Strong enrichment of T was observed in the areas covered by Be deposition layers such as the horizontal region (apron) of Tile 1 and the shadowed regions of Tiles 4 and 6 [5,6], as reported for D [7,8]. The measurements of energy spectrum of β-ray induced x-rays for the ILW-2 tiles also showed codeposition of T with Be at Tile 0 and the apron of Tile 1. Implantation of T into W layers up to depths of several micrometers was also observed at the vertical part of Tile 1 and outer upper tile (Tile 8) [9]. However, T distribution on the tiles used in ILW-3 has not been examined.

In this study, T distribution on the W-coated CFC divertor tiles retrieved after ILW-3 was measured using an IP technique and β-ray induced x-ray spectrometry (BIXS). IP measurements were performed also for ILW-2 tiles for comparison. It was found that T concentrations in Be deposition layers after ILW-3 were significantly lower than those after ILW-2.

2. Experimental procedures

The cross-sectional view of JET divertor region and tile locations are

* Corresponding author at: University of Toyoma, Gofuku 3190, Toyama 9308555 Japan.
E-mail address: hatano@ctg.u-toyama.ac.jp (Y. Hatano).
[1] See the author list of "X. Litaudon et al. 2017 *Nucl. Fusion* 57 102001".

https://doi.org/10.1016/j.nme.2019.01.001
Received 14 August 2018; Received in revised form 1 January 2019; Accepted 1 January 2019
Available online 16 January 2019

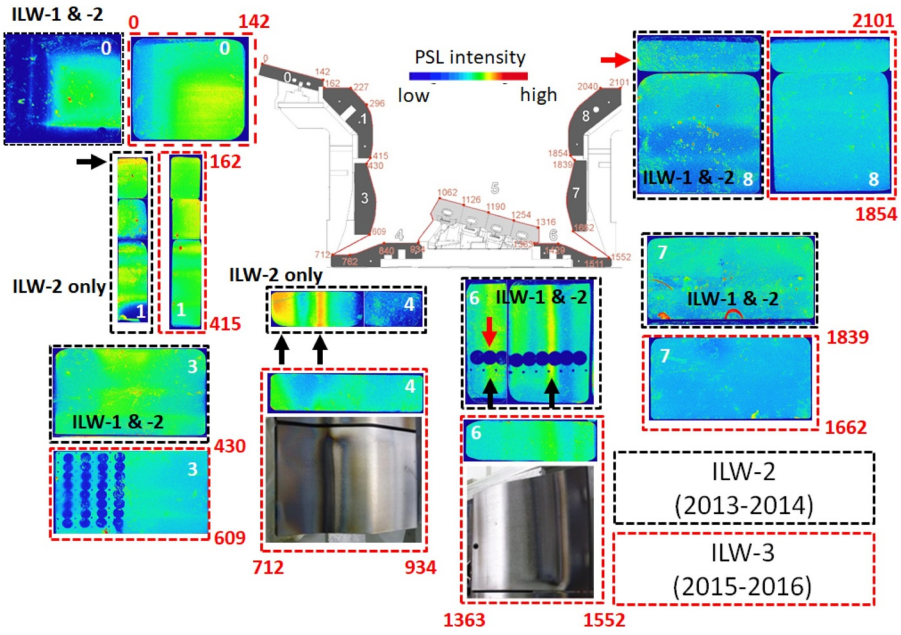

Fig. 1. Cross-sectional view of divertor region of the Joint European Torus (JET) and IP images of divertor tiles retrieved after 2013–2014 ITER-like Wall campaign (ILW-2) and 2015–2016 campaign (ILW-3). "ILW-1 & 2" means the tiles were exposed to the plasma during ILW-1 and ILW-2 and retrieved after ILW-2, and "ILW-2 only" indicate the tiles were installed in the vacuum chamber after ILW-1 and then retrieved after ILW-2.The colors indicate the intensity of photo-stimulated luminescence (PSL) from IPs in ascending order from blue (lowest), green, yellow and red (highest). Blue contrast in a round shape correspond to the area from which disk specimens were taken out by coring. Photos of Tiles 4 and 6 retrieved after ILW-3 are also shown. White letters indicate tile numbers, and red letters indicate S-coordinate corresponding to the distance along the tile surface in mm. Black arrows indicate band-like regions with tritium enrichment. Specimens corresponding to β-ray induced x-ray spectra shown in Fig. 3(a) and (b) were taken from Tiles 6 and 8 at poloidal positions indicated by red arrows.

given in the central part of Fig. 1. In this figure, white letters indicate tile number, and red letters shows S-coordinate (S) being equivalent to the distance along the tile surfaces in mm. The distribution of T on the ILW-3 tiles was examined in the VTT Technical Research Center of Finland using an IP technique in October 2017; the tiles examined were Tile 0 (tile code HFGC14N), Tile 1 (14ING1C), Tile 3 (2IWG3A), Tile 4 (2BNG4C), Tile 6 (14BNG6D), Tile 7 (14ONG7A) and Tile 8 (14ONG8A). The IP sensitive to low energy β-rays from T (BAS IP TR provided by GE Healthcare Japan Co., Japan) was used. The escape depth of β-rays from T is ~3 μm in Be and ~0.3 μm in W. After cutting into appropriate shapes, pieces of IP were wrapped with thin plastic films (1.2 and 2 μm thickness) to avoid contamination with Be and T, and then placed on the tile surfaces in the dark for 17–20 h. The retrieved IP sheets were analyzed using a laser scanner (FLA-5100, Fujifilm Co., Japan) at the University of Helsinki, and the distribution of T was obtained as intensity distribution of photo-stimulated luminescence (PSL). The size of 1 pixel was set to 100 × 100 μm. In the case of Tiles 1, 4 and 6 retrieved after ILW-3 campaign, only 1/3 of the tile surfaces were covered with IP to leave the other parts of surfaces for different types of analyses. The IP measurements for ILW-2 tiles described in [9] were conducted in August–September 2015 at the VTT. The surface of examined Tile 4 was covered by Mo layer instead of W layer to study redeposition of W [9]. Note that the majority of ILW-2 tiles examined were exposed to the plasma in JET in both ILW-1 and -2, though Tiles 1 and 4 were used solely in ILW-2 [9].

Energy spectra of β-ray induced x-rays were measured under Ar gas atmosphere for disk specimens taken by coring from the ILW-2 and ILW-3 tiles. The intensity of Ar(Kα) x-rays (2.958 keV), $I_{Ar(K\alpha)}$, indicates the concentration of T at the surface and the subsurface region within the escape depth of β-rays, and the intensity ratio of W(Lα) x-rays (8.398 keV) to W(Mα) x-rays (1.775 keV), $I_{W(L\alpha)}/I_{W(M\alpha)}$, increases with penetration depth of T into W layers due to larger escape depth of W (Lα) x-rays [9]. A silicon drift detector (SDD) with 8 μm-thick Be window (X-123SDD, Amptek Co., USA) was used. The Be window has negligible transmittance for x-rays below 0.6 keV [10]. Hence, characteristic x-rays of low atomic number elements such as Be, C and O were not able to be detected. More detailed measurement procedures are described elsewhere [9]. The spectra for the ILW-2 Tiles were obtained in January–April 2017 and those for ILW-3 tiles were acquired in January–February 2018 at the VTT.

3. Results and discussion

In Fig. 1, the IP images for the ILW-3 tiles are compared with those for the ILW-2 tiles. In this figure, "ILW-1 & 2" means the tiles were exposed to the plasma during ILW-1 and ILW-2 and retrieved after ILW-2, and "ILW-2 only" indicates the tiles were installed in the vacuum chamber after ILW-1 and then retrieved after ILW-2. The colors indicate the PSL intensity in ascending order from blue (lowest), green, yellow and red (highest). The blue contrasts in a circle shape correspond to the places from where disk specimens were taken out. In the case of the ILW-2 tiles, the band-like regions shown by yellow-red colors were observed at the apron of Tile 1, Tile 4 and Tile 6, as indicated by black arrows. The colors of these regions suggest strong enrichment of T. Similar band-like regions extended in the poloidal direction was also found for the ILW-1 tiles [5], and those regions corresponded to the areas covered with deposition layers of Be and other impurities such as C and O. Hence, the enrichment of T at these positions were ascribed to codeposition of thermalized T with Be and other impurities. However, such strong T enrichment was not observed for the ILW-3 tiles. In other words, T distribution was more uniform in the case of the ILW-3 tiles. Photos of the ILW-3 Tiles 4 and 6 are also shown in Fig. 1. The formation of deposition layers could be visually recognized as change in color from gray-silver to dark gray.

Line profiles of PSL intensity shown in Fig. 2 were generated by taking slices from 2-dimensional images along poloidal trajectory; a narrow band (2 mm width) extending in the poloidal direction was set on a plasma-facing surface of each tile, and the PSL intensity distributions in narrow bands along the poloidal direction were plotted against S-coordinate. The profile for the ILW-1 tiles [6] is also shown. The peaks of PSL intensity were observed at S = 162–173 mm (Tile 1), 712–790 mm (Tile 4) and 1363–1500 mm (Tile 6) for the ILW-1 and -2 tiles. In contrast, the ILW-3 tiles showed no clear peak and more uniform T distribution, as mentioned above. In the case of the ILW-1 and -2 tiles, the shadowed region of Tile 4 showed higher T concentration than the apron of Tile 1 though the deposition at the former was thinner than that at the latter [8]. The high T concentration at the shadowed region of Tile 4 was ascribed to high carbon to Be ratio in the deposition layer [8,11,12].

Fig. 3(a) and (b) show typical energy spectra of β-ray induced x-rays from areas with and without deposition layers, respectively. The specimens corresponding to these spectra were taken from the poloidal

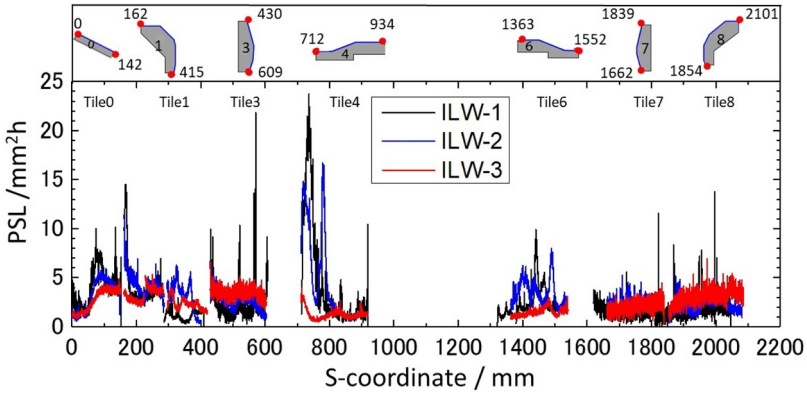

Fig. 2. Correlation between intensity of photo-stimulated luminescence (PSL) and poloidal positions (S-coordinate) for divertor tiles retrieved after ILW-1 [6], -2 and -3.

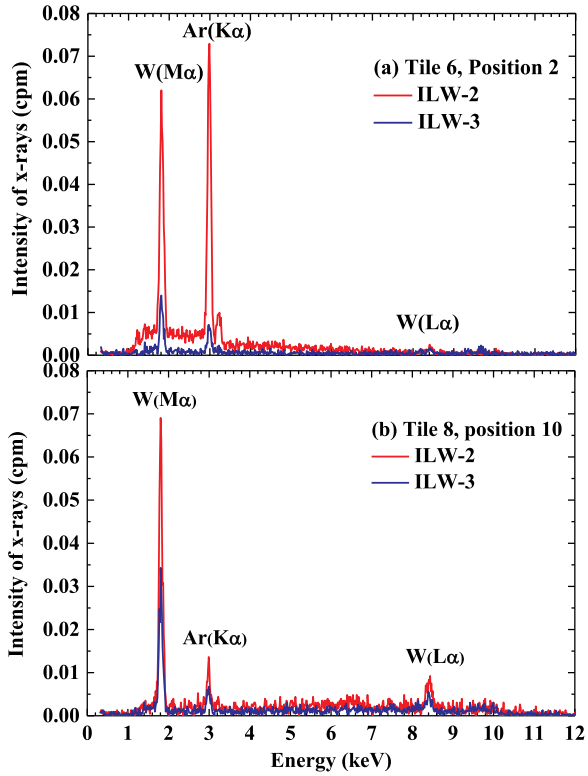

Fig. 3. Energy spectra of β-ray induced x-rays from (a) upper flat part of Tile 6 (S = 1398) and (b) horizontal part of Tile 8 (S = 2063) after ILW-2 and ILW-3 as typical examples of x-ray spectra for regions with (a) and without (b) Be deposition layers. Specimens corresponding to these spectra were taken from poloidal positions indicated by red arrows in Fig. 1.

positions indicated by red arrows in Fig. 1. The characteristics of spectra given in Fig. 3(a) (the upper flat part of Tile 6, S = 1398) are strong bremsstrahlung x-rays (the broad peak at 1–4 keV), strong Ar (Kα) and W(Mα) x-rays and negligibly weak W(Lα) x-rays. The Ar(Kα) x-rays were induced by β-rays from T present at the surface and sub-surface layers within the escape depth of β-rays, as previously mentioned. These characteristics suggest codeposition of T with Be and other impurities. The strong bremsstrahlung and Ar(Kα) x-rays relative to W(Mα) x-rays are explained by the generation of bremsstrahlung x-rays in Be deposition layers and larger escape depth of β-rays in Be than in W. The absence of Be(Kα) x-rays was due to absorption by the detector window, as described earlier. A large peak of W(Mα) x-rays shown in Fig. 3(b) (the horizontal part of Tile 8, S = 2063) together with relatively intense W(Lα) x-rays and bremsstrahlung x-rays at 4–10 keV indicate deep penetration of T into W layers (up to several micrometers) [9]. The intensity of Ar(Kα) x-rays in Fig. 3(b) is very weak compared with that of W(Mα) x-rays. The comparison of Fig. 3(a) and (b) indicates the dominant factor of the intensity of Ar(Kα) x-rays is presence or absence of Be deposition layer and T concentrations in the deposition layer.

The intensity of Ar(Kα) x-rays is plotted against S-coordinate in Fig. 4. Relatively high intensity was observed at Tile 0, Tile 1, the shadowed region of Tile 4 (S = 740–780) and Tile 6. These regions are covered by Be deposition layers [8]. The difference between ILW-2 and ILW-3 was most significant at the shadowed region of Tile 4 and Tile 6, and the intensity for the ILW-3 tiles in these regions was smaller than that for the ILW-2 tiles by a factor of 2–6. These observations are consistent with the results of IP measurements (Fig. 2), and they also suggest lower T concentrations in the deposition layers formed in ILW-3 than the case of ILW-2.

Because of longer period of operation and higher input power, it is hardly expected that the amount of T produced in ILW-3 was smaller than that in ILW-2. For the same reasons, it is improbable that the amount of Be deposited on the divertor tiles during ILW-3 was far smaller than that during ILW-2. Heinola et al. [8] compared D retention in the ILW-1 and -2 tiles and found increase in D desorption during ILW-2 plasma operation due to higher energy depositions on the tiles. Therefore, it is appropriate to consider that the lower T concentration in the deposition layers observed after ILW-3 was due to enhanced T desorption caused by higher input power than ILW-2.

Likonen et al. [13] have examined thermal desorption of D from the

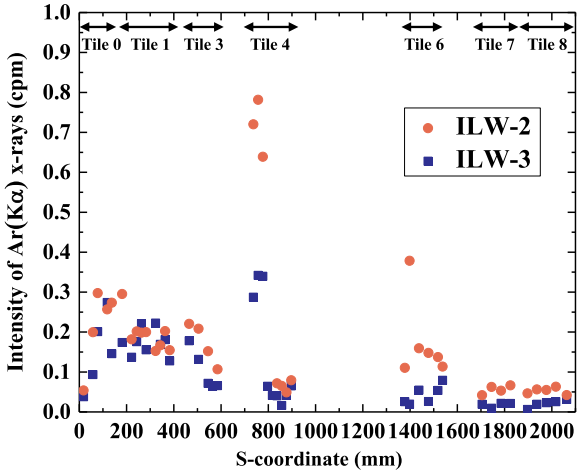

Fig. 4. Correlation between intensity of Ar(Kα) x-rays and poloidal positions (S-coordinate) for divertor tiles retrieved after ILW-2 and −3.

specimens taken from Tiles 0, 1, 3, 4 and 6 retrieved after ILW-2 and ILW-3 and reported that the desorption of HD and D_2 from ILW-3 specimens occurred at higher temperatures than that from ILW-2 specimens in most cases. Their observations indicate that the low binding energy traps were emptied during the plasma operations in ILW-3. Depth profiling of D and other elements performed in [13] using nuclear reaction analysis and secondary ion mass spectrometry showed that the amounts of impurities and the thickness of the deposition layers were comparable between ILW-2 and ILW-3 so these do not explain the differences in the release temperatures. Hence, they concluded that higher release temperatures for the ILW-3 specimens than for the corresponding ILW-2 specimens could be due to higher absorbed energies [13]. The observations for D in [13] are consistent with those for T in the present study.

4. Conclusions

The distributions of T on W-coated CFC divertor tiles used in ILW-3 were measured using an IP technique and BIXS, and compared with the distributions after ILW-2. Both techniques consistently showed that the concentration of T in Be deposition layers formed on the divertor tiles during ILW-3 was significantly lower than that after ILW-2. The lower T concentration after ILW-3 was ascribed to enhanced T desorption caused by higher energy depositions on the tiles.

Acknowledgements

This work has been carried out within the framework of the EUROfusion Consortium and has received funding from the Euratom research and training programme 2014–2018 under (Grant no. 633053). The views and opinions expressed herein do not necessarily reflect those of the European Commission. The study was supported by JSPS KAKENHI (Grant no. JP26289353), the ITER Broader Approach Activities, and the National Institute for Fusion Research (NIFS) as a part of PWI Collaboration.

Supplementary materials

Supplementary material associated with this article can be found, in the online version, at doi:10.1016/j.nme.2019.01.001.

References

[1] A. Widdowson, E. Alves, A. Baron-Wiechec, N.P. Barradas, N. Catarino, J.P. Coad, V. Corregidor, A. Garcia-Carrasco, K. Heinola, S. Koivuranta, S. Kratf, A. Lahtinen, J. Likonen, M. Mayer, P. Petersson, M. Rubel, S. Van BoxelJET Contributors, Overview of the JET ITER-like wall divertor, Nucl. Mater. Energy 12 (2017) 499–505 https://doi.org/10.1016/j.nme.2016.12.008.

[2] A. Widdowson, J.P. Coad, E. Alves, A. Baron-Wiechec, N.P. Barradas, N. Catarino, V. Corregidor, K. Heinola, A. Huber, G.F. Matthews, K. MazohataJET Contributors, Deposition of impurity metals in JET ITER-like Wall campaigns, 23rd International Conference on Plasma Surface Interactions in Controlled Fusion Devices, 17–22 June, Princeton, NJ, USA, 2018 https://psi2018.princeton.edu/abstract/index-of-accepted-abstract-authors/.

[3] M. Mayer, S. Krata, A. Baron-Wiechec, S. Brezinsek, P. Coad, Yu. Gasparyan, K. Heinola, I. Jepu, J. Likonen, P. Petersson, C. Ruset, G. de Saint-Aubin, A. WiddowsonJET Contributors, Erosion and deposition in the JET divertor during the ITER like wall campaigns, 27th IAEA Fusion Energy Conference, 22–27 October, Gandhinagar, India, 2018.

[4] P. Ström, P. Petersson, M. Rubel, E. Fortuna-Zalesna, A. Widdowson, G. SergienkoJET Contributors, Co-deposition of deuterium and impurity atoms on wall probes in the divertor of JET with ITER-like wall, 23rd International Conference on Plasma Surface Interactions in Controlled Fusion Devices, 17–22 June, Princeton, NJ, USA, 2018 https://psi2018.princeton.edu/abstract/index-of-accepted-abstract-authors/.

[5] Y. Hatano, A. Widdowson, N. Bekris, C. Ayres, A. Baron-Wiechec, J. Likonen, S. Koivuranta, J. Ikonen, K. YumizuruJET-EFDA contributors, 2D tritium distribution on tungsten tiles used in JET ITER-like wall project, J. Nucl. Mater. 463 (2015) 966–969 https://doi.org/10.1016/j.jnucmat.2014.12.041.

[6] Y. Hatano, K. Yumizuru, J. Likonen, S. Koivuranta, J. IkonenJET Contributors, Tritium distributions on tungsten and carbon tiles used in the JET divertor, Phys. Scr. T167 (2016) 014009https://doi:10.1088/0031-8949/T167/1/014009.

[7] K. Heinola, A. Widdowson, J. Likonen, E. Alves, A. Baron-Wiechec, N. Barradas, S. Brezinsek, N. Catarino, P. Coad, S. Koivuranta, G.F. Matthews, M. Mayer, P. PeterssonJET-EFDA Contributors, Fuel retention in JET ITER-Like Wall from post-mortem analysis, J. Nucl. Mater. 463 (2015) 961–965 https://doi.org/10.1016/j.jnucmat.2014.12.098.

[8] K. Heinola, A. Widdowson, J. Likonen, T. Ahlgre, E. Alves, C.F. Ayres, A. Baron-Wiechec, N. Barradas, S. Brezinsek, N. Catarino, P. Coad, C. Guillemaut, I. Jepu, S. Krat, A. Lahtinen, G.F. Matthews, M. MayerJET Contributors, Experience on divertor fuel retention after two ITER-Like Wall campaigns, Phys. Scr. T170 (2017) 014063https://doi.org/10.1088/1402-4896/aa9283.

[9] Y. Hatano, K. Yumizuru, S. Koivuranta, J. Likonen, M. Hara, M. Matsuyama, S. Masuzaki, M. Tokitani, N. Asakura, K. Isobe, T. Hayashi, A. Baron-Wiechec, A. WiddowsonJET contributors, Tritium analysis of divertor tiles used in JET ITER-like wall campaigns by means of β-ray induced x-ray spectrometry, Phys. Scr. T170 (2017) 014014https://doi.org/10.1088/1402-4896/aa8931.

[10] http://amptek.com/products/c-series-low-energy-x-ray-windows/ (Accessed 10 August 2018).

[11] M. Mayer, S. Krat, W. Van Renterghem, A. Baron-Wiechec, S. Brezinsek, I. Bykov, P. Coad, Yu. Gasparyan, K. Heinola, J. Likonen, A. Pisarev, C. Ruset, G. de Saint-Aubin, A. WiddowsonJET Contributors, Erosion and deposition in the JET divertor during the first ILW campaign, Phys. Scr. T167 (2016) 014051https://doi.org/10.1088/0031-8949/T167/1/014051.

[12] M. Tokitani, M. Miyamoto, S. Masuzaki, R. Sakamoto, Y. Oya, Y. Hatano, T. Otsuka, M. Oyaidzu, H. Kurotaki, T. Suzuki, D. Hamaguchi, K. Isobe, N. Asakura, A. Widdowson, K. Heinola, M. RubelJET Contributors, Plasma-wall interaction on the divertor tiles of JET ITER-like wall from the viewpoint of micro/nanoscopic observations, Fusion Eng. Des 116 (2017) 1–4 https://doi.org/10.1016/j.fusengdes.2018.01.051.

[13] J. Likonen, K. Heinola, A. De Backer, A. Baron-Wiechec, N. Catarino, I. Jepu, C.F. Ayres, P. Coad, G.F. Matthews, A. Widdowson, JET Contributors, Investigation of deuterium trapping and release in the JET divertor during the third ILW campaign using TDS, submitted to this proceedings.